Advances in Water Resources 72 (2014) 71–83

Contents lists available at ScienceDirect

Advances in Water Resources

journal homepage: www.elsevier.com/locate/advwatres

On cohesive sediment erosion: A first experimental study of the local processes using transparent model materials

Keang Sè Pouv [a], Anthony Besq [a], Sylvain S. Guillou [a,*], Erik A. Toorman [b]

[a] LUSAC (EA 4253), Université de Caen Basse-Normandie, Site Universitaire, BP 78, 50130 Cherbourg-Octeville, France
[b] Hydraulics Laboratory, Department of Civil Engineering, KU Leuven, Kasteelpark Arenberg 40, box 2448, B-3001 Leuven, Belgium

ARTICLE INFO

Article history:
Available online 2 June 2014

Keywords:
Erosion processes
Cohesive materials
Annular flume
Microscopic scale
Rheometry

ABSTRACT

An annular flume combined with a microscopic system is used to explore local erosion mechanisms of transparent cohesive beds (yield stress fluids) under shear-induced flowing liquid. The observations at a microscopic scale for erosion flume experiments are the originality of this work. Our first results reveal that the deformation and erosion dynamics of bed material mainly depends on its miscible state with the flume fluid, its structural organization being associated with mechanical properties and the measurement section. Shear localization within the bed is also observed. Moreover, the erosion rate and the local bed shear stress can vary with time even for an imposed constant global hydrodynamic flow as they result from the coupling between the fluid flow and cohesive bed conditions at the bottom. We also try to link the local resistance to erosion to the local cohesive strength estimated from rheometric microscopic data for the same sample conditions with homogeneous properties.

1. Introduction

In ports and estuaries, cohesive sediments, generally referred to as *muds*, are eroded in some areas and accumulated elsewhere according to hydrodynamic flow conditions controlled by various natural phenomena (*e.g.*, tide and wind) and human activities (*e.g.*, navigation). The long-term management of these privileged environments, such as prediction of perturbation due to climate change and contaminant dispersion associated with sediment, or dredging operations for navigation, requires a better understanding of sediment transport and behavior.

Numerical models are developed to simulate the sediment transport from the scale of the particle to the scale of the estuary [42,47,50,51,53–56]. It is even now not easy to provide a correct modeling for the processes related to cohesive materials [47] especially concerning the erosion of cohesive beds. Sedimentation and consolidation are processes, in which physical and chemical phenomena appear, leading to the constitution of cohesive bed. Models based on the Gibson equation [17,48,49] and on two-phase flow theory [50] have been proposed recently. Nevertheless, they are still based on the concentration, the permeability and the effective stress. The modeling of the erosion of a non-cohesive bed was studied with two-phase models [51–53] by using specific rheology models. Such a modeling remains to be done for cohesive beds. This kind of modeling needs to have a better comprehension of the processes at the local scale. For this purpose, cohesive sediment must be characterized carefully by means of experimental approaches.

A major issue of the study of sediment erosion and mechanical behavior is ascribed to its complex nature which is conditioned by a lot of factors like bulk density, salinity, organic content, mineralogical components, biological activities and mechanical history [1–3]. In addition, sediment properties vary spatially across the bed and temporally on daily to seasonal time scales [4,5]. This demands even more efforts and attention to study sediment erodibility. In this context, a large number of instruments for erosion tests, ranging from laboratory to in situ flumes, have gradually been developed [6–8]. Nevertheless, there still exists a level of uncertainty for each instrument due to a lack of standards for data interpretation and measurement methods [7,9] and due to large measurement errors [7]. The section of the sediment bed is generally designed differently from one flume to another and has an impact on the data analysis and comparison on account of the quantity of mobilized sediments [7].

For erosion tests, there are typically two inferred parameters for a time step test: the bed shear stress induced by hydrodynamic forces and the erosion rate associated with suspended sediment concentration. Different erosion thresholds can be identified macroscopically according to sediment erosion dynamics. For instance,

* Corresponding author.
E-mail address: sylvain.guillou@unicaen.fr (S.S. Guillou).

http://dx.doi.org/10.1016/j.advwatres.2014.05.012
0309-1708/© 2014 Elsevier Ltd. All rights reserved.

two thresholds have been defined by [10] and a more complex scheme related to two erosion modes (Types 1 and 2) has been reported by [11]. The Type 1, referred to as surface erosion, is firstly characterized by resuspension of recently deposited flocs, then by erosion of bed material. This ideally leads to determine two thresholds. The Type 2, known as mass or bulk erosion, corresponds to a transition to constant and continuous erosion but may represent catastrophic failure of sediment. As such, it is possible to define more than one threshold. Experimentally, it is difficult to quantify this parameter because it relies on the estimation of a "significant variation" of erosion rate for an increase of bed shear stress. The appearance of these different processes could be related to property gradients of a sediment bed (*e.g.*, density and strength) due to its structural organization. Treated natural sediments and artificial sediments (*e.g.*, bentonite and kaolinite) have also been widely studied for laboratory tests [12–14]. Although some parameters, like bulk density, can be well controlled for these materials, their internal structures are still more or less complex, and the homogeneity of bed properties also depends on the protocol used for making the bed. In spite of numerous studies on cohesive sediment erosion, no clear physical description of its mechanisms, especially the onset of material failure at micro-scale, has been reported.

Besides the difficulty in deciding on the detection and the modification of the erosion process, the estimation of bed shear stress is also delicate and can lie at the origin of variability. The four techniques commonly used to estimate bed shear stress from hydrodynamic characteristics are the following: current velocity profiles (Law of the Wall or Log Profile technique), Reynolds stress measurement, Turbulent Kinetic Energy (TKE) measurement and energy dissipation methods [15]. Kim et al. [16] have critically reviewed the suitability, assumptions and limits of these methods, and suggested that the TKE approach is best suited for either in situ or laboratory experiments.

The matter of the yielding criterion, associated with the transition between two physical states of material, reminds us of the "yield stress" concept employed in the rheological literature where the sample is usually assumed to be homogeneous. Yield stress materials are characterized by a dual behavior consisting of a solid and a liquid regime. By analogy, the erosion process can be described as a mechanical destabilization leading to a solid–liquid transition if the external force is high enough. In natural conditions, this process also includes exchange phenomena at the mud-water interface that may introduce pore water pressure gradients having repercussions on the failure process of bed material (drained or undrained failure) [17]. To our knowledge, there are only a few published papers, such as [10] and [18], describing relationships between erosion threshold and rheometric yield stress, which depend on the definitions used to determine both parameters. Typically, the critical shear stress value for erosion of soft muds is in the 0.1–2 Pa range which seems to be low as it generally concerns sediment concentrations below 1500 kg/m^3. Rheometry and erosion of sediment have mostly been studied separately. For the rheometry, a lot of works have focused on macroscopic behavior of sediment [3,19] or attempted to quantify the influence of some parameters, such as the fine fraction/coarse fraction ratio [20] and the global particle fraction [21,22], on yielding behavior.

The yield stress and the thixotropy (time-dependent behavior) are pertinent features of cohesive sediments [19,23] and generally interrelated [24], but the latter is usually overlooked in erosion studies. An important consequence of thixotropy is that the material exhibits an aging process in its solid regime. Structural organization evolves with time and consequently controls the shear stress level capable of breaking it down. A proper comparison between data of a rheometric and an erosion test can only be made if the same structural state of the sample is assured for both situations. In all cases, the initial state of the sample should be as well controlled as possible [25,26].

Recent studies have given a wide vision of the rheological behavior of yield stress fluids regardless of their nature (*e.g.*, emulsions, gels and cohesive sediments) and physical origin of structural organization (*e.g.*, steric effects and interactions) [24,27]. Flow homogeneity is a crucial aspect of these materials [28,29]. The solid–liquid transition, defined by a transition time corresponding to the minimum of the deformation rate evolution [30], or to a homogenous shear steady state [31], depends on the applied stress. For simple (non-thixotropic) yield stress fluids (*e.g.*, repulsive concentrated emulsions and purely aqueous carbopol gels), a steady homogeneous flow is obtained when applied stress exceeds the yield stress, in other words all shear rate values can be explored in the flow regime. Nevertheless, shear banding is not excluded during a transient regime [31]. For thixotropic yield stress fluids (*e.g.*, clay suspensions and granular materials), there exists a critical stress associated with a critical shear rate, below which, the material cannot attain a homogeneous steady-state behavior. For an imposed stress higher than the yield stress, the solid–liquid transition takes place in such a way that the sheared zone grows with time until it reaches the total volume of the sample. These observations underline the importance of a local approach for interpreting or correcting macroscopic data. In addition, the flow behavior depends on experimental conditions, such as controlled shear stress or controlled shear rate [19,32]. Thus, there exists a range of "apparent" data of flow curves, and it is delicate to give physical meanings to parameters (*e.g.*, yield stress) of models describing this apparent domain (*e.g.*, Dual-Bingham and Worrall–Tuliani models [22]).

For erosion studies, a local approach seems to be mandatory to investigate eventual heterogeneity of a sediment bed and to capture the deformation's evolution during solid–liquid transition dynamics even prior to the bed's breaking off. These processes can be studied quantitatively for tests with or without exchanges at the bed interface as this aspect could lead to more or less important bed perturbations even if there is no flow. If the same approach is applied to rheometric tests, it is possible to find correlations between both types of experiments via local transition behavior of reproducible samples, and estimate, in an indirect way, the bed shear stress value.

In this paper, local processes of cohesive bed in an annular flume are explored using a particle imaging tracking technique. Since transparent bed materials are required for this optical technique, two aqueous materials mimicking cohesive sediments were specifically prepared so as to obtain close yield stress values and different thixotropic levels. This allows us to quantify the influence of these parameters on the erosion behavior. Exchange phenomena at the bottom are considered by using three kinds of driving liquid which are miscible or not with the two aqueous bed materials. The effect of measurement section is also explored. In the end, results of these tests are discussed and some of them are correlated with those of local observations during rheometric creep tests.

2. Materials

2.1. Bed materials

Two transparent model systems were prepared using two well-known commercial rheology modifiers, namely, carbopol Ultrez 21 (Noveon) and laponite RD (Rockwood Additives). Carbopol is a polymer elaborated from cross-linked linear polyacrylic acid chains and usually used as a thickener [25]. It is delivered in the form of more or less agglomerated and polydisperse particles with the typical size of roughly a few microns [41]. An acid dispersion is obtained when the resin is mixed with pure water. Adding an appropriate quantity of a suitable base leads to elaborate a neutralized gel which is the result of the assembly of microgels filled with solvent [25]. This structure is inhomogeneous at microscopic scale. Depending on carbopol concentration, microgels occupy more or less space and could not be totally swollen [33], which thus leads to a high or a low yield stress value. Carbopol gels are generally known as simple yield stress fluids [29]. Laponite is synthetic clay having similar composition and structure to natural hectorite of the smectic group [34,35]. It is delivered in the form of white colloidal particles with a thickness of 1 nm and a diameter of 25 nm [34]. By varying a few parameters, such as concentration and ionic strength, the laponite suspension can be turned into different states like Newtonian liquid, viscoelastic gel or elastic solid [36].

The first model material was an aqueous carbopol gel. It was prepared by dispersing carbopol powder (0.3 wt.%) in ultrapure water (Chromasolv 34877, Sigma Aldrich) (14.45 wt.%) using a magnetic stirrer (at 500 rpm for 20 min). Then, glycerol (VWR International) (85 wt.%) was added into the mixture and stirred at 1100 rpm for 20 min. This component was used to increase the density and refractive index of the system required for future works on gel–PMMA beads systems in an attempt to mimic cohesive sediment–sand mixtures. After a rest time of 20 min, allowing carbopol particles to hydrate and swell freely in the solution, the system was neutralized by adding triethanolamine (Fluka 90280, Sigma Aldrich) (0.25 wt.%) and mixing manually with a metal spatula until the gel became visibly homogeneous (about 20–30 min). In order to limit aging effects and obtain reproducible properties, the gel was homogenized the following day using a dispersing machine (Ultra-Turrax) (at 11,000 rpm for 2 min). Then, a centrifugal process was executed (at 5000 rpm for 20 min) in order to expel air bubbles. Finally, a carbopol gel (pH $\approx$ 7) with a density of 1223 kg/m^3 and a refractive index of 1.446 was obtained.

The second model material was an aqueous mixed laponite–carbopol gel. At first, a water–laponite dispersion at 2 wt.%, and a water–NaCl (S/3160/53, Fisher Scientific) solution at 2×10^{-3} mol/l, with an equal volume, were prepared separately, then left hydrated for one day before entirely mixing together to achieve a new system at 1 wt.% and 10^{-3} mol/l. Then a carbopol gel at 0.3 wt.% was prepared using the above protocol up to the homogenizing step. After two days, the mixed system (45.9 wt.%), the carbopol gel (39.1 wt.%) and glycerol (15 wt.%) were dispersed at 11,000 rpm for 2 min. After completing the centrifugal process (at 5000 rpm for 3 min), a mixed laponite–carbopol gel (pH $\approx$ 7.8) with a density of 1153 kg/m^3 and a refractive index of 1.392 was achieved.

Both transparent gels were seeded with dried melamine particles (2.81 ± 0.14 μm diameter, Granuloshop) at a very low concentration of 1000 particles/mm^3 which does not affect the material properties. These particles will be later tracked in order to probe local deformation/flow of the material.

The flow behaviors of these two transparent materials were characterized by means of a controlled-stress rheometer (RheoScope1, Thermo Fisher Scientific) equipped with a rough plate/plate geometry of 28 mm diameter. The apparent gap was fixed at 1 mm. The initial state of the sample was controlled by a cyclic preshear at a constant shear rate of 1 s^{-1} for 90 s followed by a rest time of 120 s. By using controlled-stress linear ramp tests with a sweep rate of 0.067 Pa/s, we obtain the flow curves characterizing shear-thinning and visco-plastic behaviors (Fig. 1). For low shear rate values (<0.005 s^{-1}), the upward flow curves of both gels are superimposed. This apparently suggests that both materials present similar elastic solid responses and close yield stress values ($\approx$16 Pa). It should be reminded that the part of the flow curve around the yielding transition depends on the sweep rate of applied stress [37]. Creep experiments for the same two gels [3]

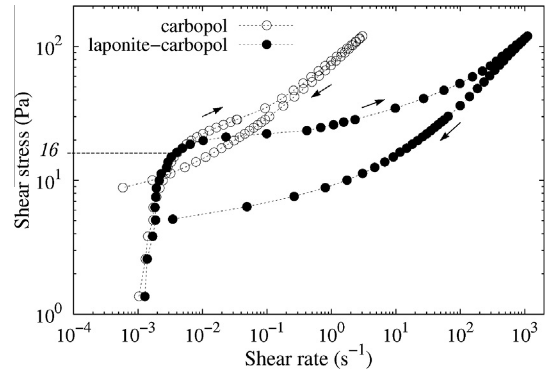

Fig. 1. Flow curves of the two gels obtained by using controlled-stress linear ramp tests.

have revealed that the transition time leading to flow regime could be defined for a stress range with a minimal value $\tau_{\min}$, and evolves exponentially with the inverse of shear stress: $t_c = a.\exp(b/\tau)$. This relationship is also obtained for other yield stress fluids [30]. The values of a, b and $\tau_{\min}$ for the two gels are shown in Table 1. The laponite–carbopol gel presents a slightly lower yielding value and a more brittle behavior (smaller a value). This observation is consistent with the presence of a larger shear stress plateau of the upward flow curve above the yield stress. Local observations have proved that shear localization occurs in this regime [38]. Such feature seems to be a hallmark of time-dependent materials [28,29].

The hysteresis loop of flow curves is a characteristic of time-dependent material which strongly depends on their flow history. Both solid–liquid and liquid–solid transitions, leading to define respectively the static and the dynamic yield stress [23], can be defined. The static yield stress increases with rest time whereas the dynamic yield stress corresponds to the lowest stress value that can be reached in a homogeneous steady-state flow. Fig. 1 reveals that the thixotropy exists for both materials and is much more pronounced for the system containing clay particles (larger hysteresis loop). Since it is accepted that purely aqueous carbopol gels are simple yield stress fluids [25,29], the peculiar weak thixotropy of our carbopol gel could be ascribed to the presence of glycerol. Furthermore, we checked that the values of the elastic modulus G' and the viscous modulus G'' of the laponite–carbopol gel (50 Pa and 7 Pa) are smaller than those of the carbopol gel (90 Pa and 35 Pa).

It is obvious that both systems, made mainly of polymer molecules, still cannot represent real cohesive sediments in terms of the internal structures which control the resistance to erosion. However, it has been shown that the rheological behaviors (*i.e.*, flow behaviors, solid–liquid transition and aging dynamics) of both materials are similar to the ones of some cohesive sediment [3]. Moreover, their transparent feature enables us to use an optical technique to analyze the local processes from the deformation to the erosion step, which makes it possible to identify better the onset of erosion.

Table 1
Characteristic parameters obtained with creep experiments for the two gels [3].

Gel	a (s)	b (Pa)	$\tau_{\min}$ (Pa)
Carbopol	0.021	195.5	16
Laponite–carbopol	0.001	195.5	14

2.2. Flume fluids

Three different kinds of driving fluid including tap water–glycerol solution (87.5 wt.%–12.5 wt.%), commercial white spirit (Notilia) and white spirit–paraffin oil (Sigma Aldrich) solution (50 wt.%–50 wt.%) were used. Afterwards, these three Newtonian fluids will be designated as W-G, WS and WS-PO, respectively. Their density ρ and kinematic viscosity υ values at 19 °C are shown in Table 2. For the sake of velocity measurement using Particle Image Velocimetry (P.I.V.), all the fluids were seeded with hollow glass particles (10 µm diameter, Dantec Dynamics). Amongst the three fluids, only the W-G system is miscible with the above formulated aqueous gels.

3. Erosion experiments

3.1. Experimental system

The erosion experiments were conducted using a system consisting of a PMMA mini annular flume, a P.I.V. system (LaVision) and a microscopic device (RheoScope1, Thermo Fisher Scientific) (Fig. 2a). Annular flumes are considered as systems capable of reproducing flow conditions that are comparable to those experienced by sediments under calm, wave-free condition in estuarine environment [15].

The flume has a circular channel with an inner radius of 114.5 mm and a width of 35 mm. The flow within the flume is generated by the rotation of the top ring controlled by setting the torque shaft value (Rheoscope 1). The depth of the fluid near the outer wall is 62.5 mm. The inclination of the surface of the ring in contact with the fluid was designed to obtain a constant shear velocity in the laminar regime. The aluminum bottom plate of the flume is horizontal and contains a shallow channel (2 mm depth and 37 mm width) to be filled with sediment alone (total section bed, Fig. 2b) or sediment together with a series of solid plates (partial section bed, Fig. 2c). Our experimental system is similar to the one reported in [39] but the range of the ring rotating speed of our system (8–19 rad/s) is nearly 4 times lower.

The microscopic device (lens 5X, magnification factor = 1.193 µm/pixel) underneath the flume was used to record series of images of a sediment volume (764 µm × 573 µm × 60 µm) during the tests (zone 1). The position of the focused zone could be adjusted during the test. It was thus possible to track the evolution of bed thickness due to erosion. The image acquisition frequency was adjusted according to tracer particle dynamics (typically, 4 image/s for the first period of 300 s and 0.1 image/s for the rest). The ImageJ software and the associated Particle Detector & Tracker plug-in [40] were employed to exploit series of images in order to determine temporal 2D coordinates of tracer particles required for analyzing local dynamics of transparent cohesive bed. The same microscopic device and particle tracking technique were also used to study the local behavior of the same materials within parallel plates for rheometric experiments [38].

2D Velocity field of fluid nearby the bed was measured using the P.I.V. system (zone 2). Two 45° inclined mirrors enable us to adjust the position of the horizontal laser sheet. The CCD camera was fixed vertically above the flume to capture, at each pulsation, images (54 mm × 41 mm) of the illuminated fluid layer. Five visualization planes at different heights above the bed (z_f = 0.3; 1.88; 3.45; 5.02 and 6.60 mm) were fixed for velocity measurements. For each plane, 510 pairs of image were recorded. The acquisition was started after 10 min from the start-up which ensure a steady-state turbulent regime (Fig. 3). The number of recorded images is large enough to provide significant statistical data of velocity parameters including the average and the RMS. The velocity fields in the Cartesian coordinates (u_x, u_y) calculated by the Davis software (multipass intercorrelation algorithm with a "nil velocities" mask for the solid parts) were used to be interpolated on a regular polar mesh with the origin at the rotation center of the flume. This allows us to obtain the velocity fields in the Polar coordinates (u_r, u_θ) where the component u_θ corresponds to the principal direction of the flow. This procedure was conducted using a code written in Scilab software.

Table 2
Density and kinematic viscosity values of the three driving fluids at 19 °C.

Driving fluid	ρ (kg/m^3)	υ (m^2/s)
W-G	1021	1.54 10^{-6}
WS	770	1.50 10^{-6}
WS-PO	821	7.50 10^{-6}

3.2. Protocol

Two sediment sections (TS and PS) with the same thickness of about 2 mm but different forms and sizes were taken into account (Fig. 2b and c). Concerning the TS type, the whole shallow channel of the bottom plate was first covered with sand paper (roughness of the order of 35 µm) to avoid the wall slip then filled with the sediment. As for the PS type, the shallow channel was filled with a series of smooth rigid solid plates, knowing that one of them was cored circularly for pouring the sample.

As the material behavior is mechanically affected during the loading into the cell, a shearing step was applied in order to control the initial state of the sample as much as possible. For the TS type, the sample was sheared using a smooth rigid disc by moving it clockwise and then counterclockwise at a rate of ±1 rpm for 300 s. For the PS type, the preshear consisted in scraping the sediment surface radially then tangentially (one time for each). After this conditioning step, the inner solid cylinder and the outer hollow box were coaxially assembled on the bottom plate to form the annular flume. Then, the channel was filled slowly and carefully in order to minimize bed disturbances, especially around the zones 1 and 2. As the set up time after shearing until experiment start up was fixed, a reproducible initial state of bed material was to be obtained.

The temperature of the room, where all the samples were stocked and the measurements were carried out, was maintained at 17 ± 0.15 °C.

Since we have two bed materials, three kinds of fluid and two bed sections, many experiments could be conducted to investigate various effects on the erosion (Table 3). The tests with exchanges at the bed interface (*i.e.*, when W-G system which is miscible with bed materials is used) are more relevant for natural conditions. For the tests with the immiscible fluids, the homogeneity of the bed material is preserved and only drag and interfacial forces induce bed deformation. If we think of natural conditions, these tests can be related to a much consolidated bed because the mechanical strength of the bed is very high. Moreover, the non-exchanges between the bed material and the fluid which keeps the initial bed properties unchanged allow us to better analyze the influence of different parameters (*i.e.*, thixotropy, bed section, turbulent regime and fluid viscosity) on the erosion. Thus, they allow a complementary approach of erosion phenomena which has not yet been examined, and of multi-fluid flows which has received more attention (such as visco-plastic lubrication [44,45]). In natural conditions, the total sediment section can represent the case that the sediment bed has the same properties under a flow condition, whereas the partial bed section can be considered as a mixture between a non erodible and an erodible sediment bed. The main reason that we investigate these two different

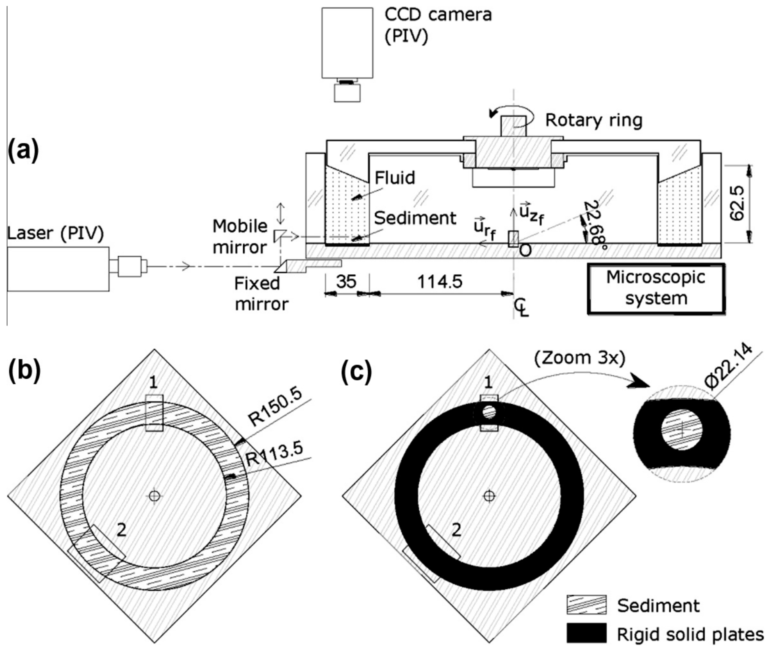

Fig. 2. (a) Schematic system for erosion flume tests, (b) and (c) TS (total section, 30700 mm^2) and PS (partial section, 385 mm^2) sediment beds, respectively. The length unit used is *mm*. The zones 1 and 2 are where local sediment dynamics and driving fluid flow are studied, respectively.

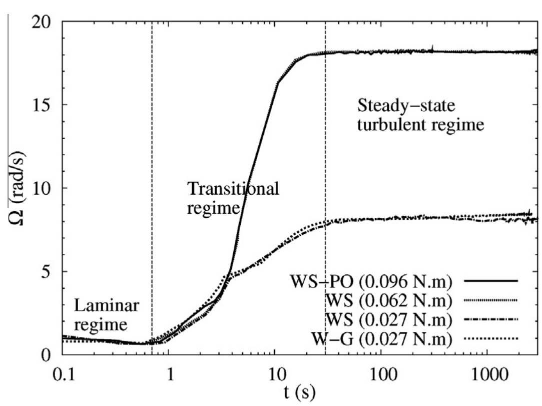

Fig. 3. Temporal evolutions of the ring rotating speed for different driving liquids and applied torques. In the steady-state turbulent regime, the Reynolds number is around 14,700 for the WS-PO (0.096 N.m), 73,900 for the WS (0.062 N.m), 32,800 for the WS (0.027 N.m) and 32,200 for the W-G (0.027 N.m). In the laminar regime, the Reynolds numbers for all the tests are smaller than 2000.

sections is that we use the same erosion flume which allows a more reasonable comparison between sections. It also allows us to see how the effect of the design of measurement section has on the experimental results can be. This point is important because many erosion flumes were developed with different bed sections and measurement techniques, which makes it difficult to compare the results between them as there may exist a level of uncertainty for each instrument.

Each test was carried out by applying a constant torque with time. The temporal evolutions of the ring rotating speed Ω for different cases are illustrated in Fig. 3. The WS was used for the tests with the PS carbopol bed while the W-G and WS-PO systems were employed for the tests with the two gels and the two types of bed section. We checked that Ω does not depend on the type of the bed. During the first 3 s, we observe almost the same evolution for all the tests. After that, the rotating speed increases more or less sharply depending on the imposed torque before stabilizing after about 20 s for the two highest torque values and 30 s for the lowest torque value. Basing ourselves on the Reynolds numbers determined from Ω values and ring radius, we can distinguish different flow regimes developing during the tests as illustrated. We will later show that these regimes are related to local sediment dynamics.

3.3. Radial position for local observations of transparent cohesive bed

Since this study aims at having a broad view of local processes of cohesive bed, only one zone was focused on. This zone should present the maximal bed shear stress which could be identified

Table 3
Experiments.

Test	Exchanges at the bed interface	Fluid	Re	Bed section	Bed material
1	Yes	W-G	32,200	TS	Carbopol
2	Yes	W-G	32,200	PS	Carbopol
3	Yes	W-G	32,200	TS	Laponite–Carbopol
4	Yes	W-G	32,200	PS	Laponite–Carbopol
5	No	WS	32,800	PS	Carbopol
6	No	WS	73,900	PS	Carbopol
7	No	WS-PO	14,700	PS	Carbopol
8	No	WS-PO	14,700	TS	Carbopol
9	No	WS-PO	14,700	PS	Laponite–Carbopol
10	No	WS-PO	14,700	TS	Laponite–Carbopol

from the velocity field of flume fluid near the bed. Thus, its radial position r_f had to be fixed. Since our main objective is not to characterize hydrodynamic flow which is complex due to the annular form, we opt to analyze only the average tangential and radial velocity.

Fig. 4 illustrates the results of the tests without bed material erosion, thus no flow disturbances due to matter in suspension or bed interface changes. The maximum velocities appear in the 135–145 mm radial position range. The two tests with the WS-PO (Re_3) present the highest maximum tangential velocity. They are close to the ones for the WS (Re_2) experiment as ring rotating speed is the same (18 rad/s). Nevertheless, the flow situations (mainly close to the walls) observed in the vicinity of the bottom clearly depend on the interaction between fluid and bed characteristics (section, material). As maximum tangential velocity correspond to different radial position range, we decided to investigate local dynamics of cohesive bed at r_f = 139.5 mm where both velocity component will contribute to an important bottom shear stress.

3.4. Bed shear stress

With our current experimental set-up, we cannot estimate the bed shear stress from the shear velocity (law of the wall approach) because we checked that the spatial resolution imposed by the laser sheet thickness (PIV) is not sufficient. Since the fluctuating vertical component of velocity was not measured, the turbulent kinetic energy method could not be used either. Finally, we opt to estimate the local bed shear stress in an indirect way by comparing local deformation rate between flume measurements and rheometric creep tests. This correlation will be presented in the Section 4.3.

4. Results

4.1. Experiments with exchanges at bed interface

For all the tests presented in this part (Re = 32,200), the W-G solution, which is miscible with the two bed materials, was employed. For each test, the horizontal visualization window was located at r_f = 139.5 mm and close to the bed surface. In order to observe the evolution of local bed thickness, the vertical position was adapted according to the erosion with time.

Two series of images, showing local structure evolution of the TS carbopol bed and the TS laponite–carbopol bed during early periods of the tests, are presented in Fig. 5. At this scale, we see

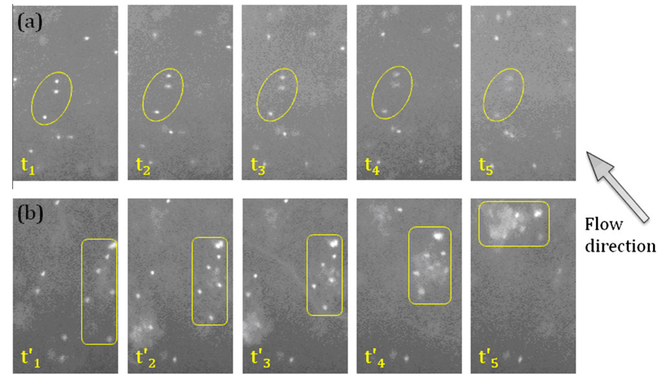

Fig. 5. Particle dynamics within a fixed visualization window during early periods: (a) TS carbopol bed, (b) TS laponite–carbopol bed. The size of each image is 143.14 μm × 238.60 μm. The total durations from t_1 to t_5 and t'_1 to t'_5 are respectively 340 s and 34 s. All the particles in the frames are immediately pulled up from the bed just after the instants t_5 and t'_5.

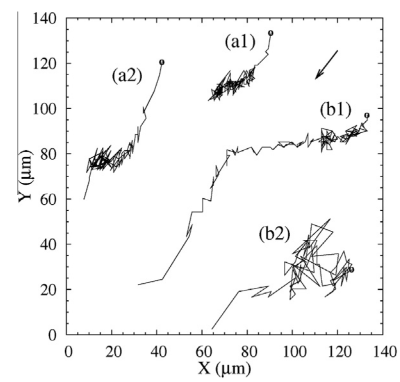

Fig. 6. Particle trajectories during early periods of four different tests: (a1) TS and (a2) PS carbopol beds, (b1) TS and (b2) PS laponite–carbopol beds. The durations of the four particle trajectories (a1, a2, b1 and b2) are respectively 784 s, 456 s, 197 s and 138 s. The particles are immediately pulled up from the bottom just after these moments. The arrow indicates the principal direction of the current at the visualization scale. The origin (o) of each particle is fixed arbitrarily.

that the bed surface presents a clustered organization. During a first short period, similar processes are observed for the same bed material irrespective of its section. The tracers trapped in a cluster become more and more blurred with time due to modifications of bed material properties by interaction with the liquid. For the carbopol gel (Fig. 5a), it does not seem that all the tracers migrate remarkably before they are individually pulled up and transported by the current. Thus microstructures at the bed surface are eroded more directly and continuously in a similar way to "stripping". For the mixed gel (Fig. 5b), the erosion is much faster. The stripping process also exists but another one described as "cluster fragmentation" dominate. Collective displacement of tracers reveals the separation and deformation of a cluster which is then pulled up and transported by the current (*i.e.*, rupture of inter-cluster bonds). The average size of the clusters is about 75 μm. The presence of the laponite clay in the system is at the main origin of aggregate formation as this phenomenon does not occur for the pure carbopol gel. In addition to these two processes, "mass erosion" was also observed at the final step of this test as the final layer of the bed with a thickness of about 0.6 mm was brutally eroded (see Fig. 7 for the temporal evolution of the bed thickness). Thus, erosion mechanisms, which cannot be clearly seen macroscopically, mainly depend on structural organization of the bed. The presence of various erosion processes suggests that there

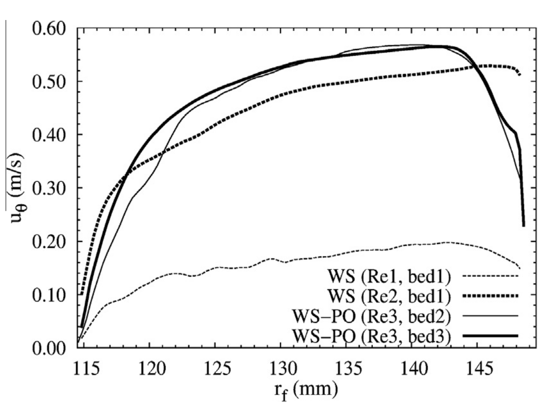

Fig. 4. Tangential velocity profiles at z_f = 0.30 mm for different experimental conditions ($Re1$ = 32,800, $Re2$ = 73,900, $Re3$ = 14,700, bed1 = PS carbopol bed, bed2 = TS carbopol bed, and bed3 = TS laponite–carbopol bed). The inner and outer walls of the flume are located at r_f = 114.5 mm and 149.5 mm, respectively.

exists more than one threshold as similarly reported elsewhere [10,11] for natural sediments. Moreover, the rapid erosion highlights that the bottom shear stress is much greater than the local strength of the bed.

In order to quantify local dynamics of cohesive bed before failure occurs, it is interesting to analyze particle trajectories reconstructed from series of images recorded during early periods of four tests with different materials (carbopol and laponite–carbopol gels) and bed sections (PS and TS beds). For each test, only the data of one selected tracer are discussed (Fig. 6). The particle trajectories within the two carbopol beds look similar but their sizes are different. At first, the particle moves in a similar direction as the current but seems to slow down with time. Then, it displaces randomly around a principal path, deviated from the previous direction towards the inner wall of the flume, before brutally taking off from the bed by the flow. The particle random displacements before the break-off are associated with the elastic response of the carbopol gel under the external forcing and structural modifications due to the miscibility with the flume fluid. Regarding the laponite–carbopol gel, particle dynamics are faster and more complex. Hence, the presented particle trajectories are not so typical since they can be completely different from one place to another as seen in Fig. 6b. For the TS bed, particle motions during the very first period are similar to what observed in the carbopol beds. After that, the particle displaces more regularly in a specific direction then in another one parallel to the current (cluster formation and deformation induced by the current) before it is eroded brutally. For the PS bed, the modification of bed surface structures due to their early exchanges with the fluid did not allow us to observe direct particle displacements during the very first time of the test. However, the recorded data show that the particle migrates randomly and strongly in an area, than in another one before displacing in the same direction as the current. Providing the difference of the durations of particle dynamics for the four tests, the erosion is more critical for the PS bed and for the laponite–carbopol gel.

As gradual erosion of the material implies the adjustment of the focus at the top of the bed with time, we can use this value to assess the temporal evolutions of the bed thickness e_f and the erosion rate E (Fig. 7). Indeed, disturbances at the bed interface took place during the filling of the flume with W-G solution and at rest until flow start up. As such, the first vertical position of the first observation zone at $t = 0$ s does not correspond to the localization of bed interface which is diffuse. This effect is more important for a flume section totally filled with gel.

In Fig. 7, we observe that each evolution of the bed thickness exhibits at least two steps. The first one, characterized by a slight decrease of the bed thickness with time, corresponds to the erosion process of the initial bed layer shown in Figs. 5 and 6. For the second one, the thickness reduces more rapidly and almost regularly with time. We found that erosion mechanisms during these two stages are similar although the erosion rates are different. The third stage only occurs for the laponite–carbopol gel. This specific process, corresponding to the brutal removal of the whole remaining bed (*i.e.*, $e_f \approx 0.65$ mm and 1.1 mm for the TS and PS laponite–carbopol beds, respectively), is described as mass erosion. The duration of the total erosion is longer for the carbopol gel than for the mixed gel and for the TS bed than for the PS bed. Thus, the erosion does not only depend on apparent hydrodynamic flow conditions but also on the nature and topography of the cohesive bed. In other words, the bed conditions and fluid situations are interdependent.

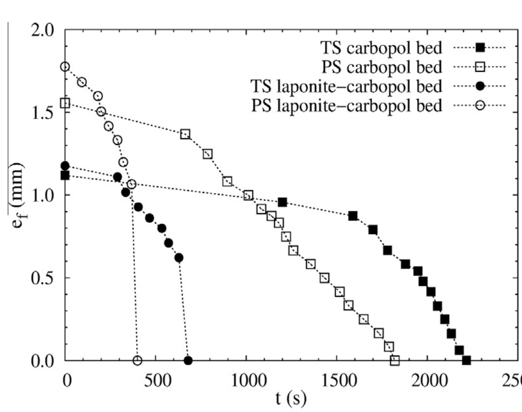

Fig. 7. Temporal evolution of the bed thickness.

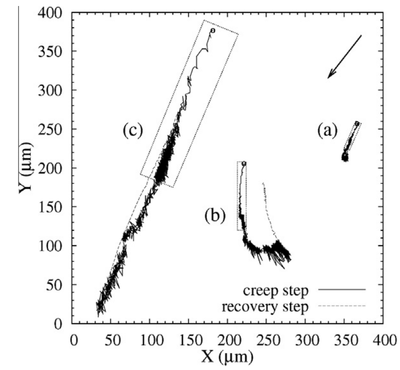

Fig. 8. Particle trajectories during three different tests with the same PS carbopol bed: (a) WS at $Re = 32800$, (b) WS at $Re = 73{,}900$ and (c) WS-PO at $Re = 14{,}700$. The durations of the creep and the recovery step of these tests are respectively 10300 s & 1900 s, 10300 s & 200 s and 5700 s & 3500 s. The dotted frames present the data obtained during the first 300 s of the tests, for which the recording rate is 4 image/s. After that, the recording rate is 0.1 image/s. The arrow indicates the principal direction of the current at the visualization scale. The origin (o) of each particle is fixed arbitrarily.

By supposing that the cohesive bed thickness in the section uniformly evolves with time, standardized erosion rate could be estimated by considering:

$$E = -\rho \frac{e_f(t) - e_f(t_0)}{t - t_0} \tag{4}$$

where $e_f(t)$ is the local bed thickness at time t, and $e_f(t_0)$ is the initial local bed thickness at time t_0. Since the erosion rate is correlated to the bed thickness, it is not important to present its evolution. However, we checked that the erosion rate values are of the same order of magnitude as those reported for some erosion tests with concentration measurements [7]. Fig. 7 also underlines the importance of the duration of mechanical solicitation. In addition, the decision on the occurrence of erosion by traditionally basing on the estimation of a significant increase of the erosion rate for an increase of the bed shear stress seems to be tricky as local processes of sediment could already take place earlier. In many erosion flume tests, erosion rate is based on measurements of concentration at some distance above the bed, while the first eroded particles remain loose on the bed (like our gels) and are transported as bed load and remain undetected by the concentration probe.

4.2. Experiments without exchanges at bed interface

By using water-immiscible driving fluids (WS and WS-PO), the bed intrinsic properties remain unchanged and the bed thickness remains constant ($e_f \approx 2$ mm, practically) before flow start-up. No mass exchanges inside the bed occur during the test. The local observation zone is located at $r_f = 139.5$ mm and $z_f = 1.9$ mm (about

0.1 mm below the bed surface owing to technical limits of the microscope).

4.2.1. Effects of fluid characteristics

In order to investigate the effects of turbulent regime and viscosity of the driving liquid, we performed three tests using the same PS carbopol bed and different fluid flow conditions: (a) WS at $Re = 32800$, (b) WS at $Re = 73900$ and (c) WS-PO at $Re = 14700$. For each test, we examine the local response of the cohesive bed during the rotation of the top ring (creep step), and continuously after it is stopped (recovery step).

For all these situations, we checked that all particle trajectories observed simultaneously in a fixed visualization window are mostly very similar. The typical particle trajectories obtained at the same location for the three tests are illustrated in Fig. 8. Overall, particle motions during the first period of each test, associated with the turbulent flow regime onset, are very similar to those shown earlier when the W-G system was employed as fluid. Then, the particle migrates randomly and very quickly around each position while it advances slowly in a principal direction. Such dynamics are due to the coupling between the mechanical strength of bed material and the fluctuating component of bottom shear stress. For both tests with the WS, the particle displacement becomes mostly transverse to the current after a certain time. On the other hand, the particle naturally moves over a longer distance when the Reynolds number is higher. Since the bed shear stress also is proportional to the viscosity of driving fluid, the particle displacement induced by the WS-PO system, which is more viscous than the WS (*i.e.*, smaller Reynolds number for the same flow velocity), is greater. Nonetheless, no material is eroded for these tests although the induced current is much more powerful than the one generated during the previous tests with the water-miscible fluid. This implies that the bed shear stress is smaller than the yield stress of the cohesive bed and only able to deform it elastically.

During the recovery step, the particle immediately move backwards, in a direction parallel to the one tracked during the shearing (creep) step, due to the elasticity of bed material. At first, it moves very fast then progressively slows down without any random dynamics. The further the particle displaces during the creep step, the further it goes back during the recovery step. However, it does not seem that the particle could reach its initial position, which indicates that some damage (*i.e.*, micro-cracks) is caused to the bed structure (soil skeleton).

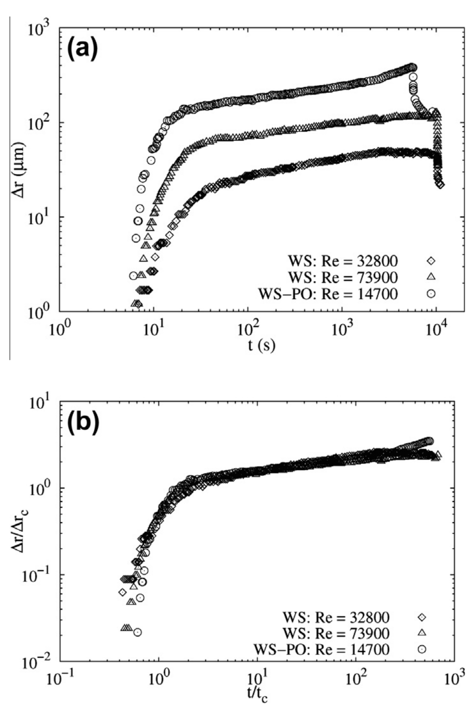

Fig. 9. (a) Temporal evolution of the particle displacement from its initial position during the creep and recovery steps, (b) non dimensional particle displacement profiles during the creep step.

As particle motions probe the local strain of the material during these tests, it is worth quantifying it.

Fig. 9a presents the temporal evolutions of the particle displacement compared to its initial position ($\Delta r = \sqrt{(x_i - x_0)^2 + (y_i - y_0)^2}$ where (x_0, y_0) and (x_i, y_i) are respectively the coordinates of particle's positions at the initial time t_0 and the time t_i) which corresponds to a creep/recovery curve. In order to limit fluctuant values due to particle random motions, only the data with the condition of $\Delta r(t_i) > \Delta r(t_{i-1})$ are plotted. Each profile depicts globally four phases during the shearing step. The first and third phases are respectively characterized by a rapid and a slow increase of the displacement with time (power law evolutions) while the second is the transitional phase between them. These phases seem to be typical for all the tests and advocate the viscoelastic behavior of bed material under shear. The first two phases are related to the flow onset regime, consisting of laminar and transitional phases, near the bottom of the flume. As such, the total duration of these two phases (≈20 s for the WS-PO, 30 s and 40 s for the WS at the higher and the lower Re, respectively) is considered as the characteristic time of flow onset t_{co} as it is also close to what observed on the evolutions of the ring rotation speed (Fig. 3). It takes more time for the WS to have a steady state flow regime at the bottom compared to the more viscous WS-PO. For each test with the WS, the last phase is materialized by a plateau of Δr related to the change of particle direction starting at about 2000 s and 4000 s for the lower and the higher Re, respectively. These are signs of material aging behavior in elastic domain under small bed shear stress, *i.e.*, the viscosity increases in time [46]. For the test with the WS-PO, the particle displacement increases slightly sharper during the final phase starting at about 2500 s. This could correspond to the start up of the solid–liquid transition of the gel. During the recovery step, the same phenomenon occurs for all the tests as the displacement decreases drastically during the first short period then much more slowly. The duration is too short to estimate the strain recovery ratio. Similar trends have also been observed in rheometric studies for a kaolin suspension and carbopol gels at various concentrations [41]. The distribution of bonding strength influences creep and recovery responses, and implies a clear distinction in viscoelastic behavior between solid and fluid states.

The non dimensional evolutions of the particle displacement shown in Fig. 9b are obtained by using the coordinates of the intersection point (t_c, Δr_c) between the two lines extrapolated from the first and the third phase of each profile in Fig. 9a. The characteristic time t_c is thus smaller than t_{co}. Overall, all the curves are well superimposed until a certain time, which reveals similar response of the bed material under different flow conditions. After that, the dimensionless displacement either increases slightly stronger (test with the WS-PO) or remains constant (tests with the WS) according to the competition between the local shear stress and the mechanical strength of the sample.

4.2.2. Effects of bed characteristics

Four creep tests with the same fluid flow condition (WS-PO at $Re = 14{,}700$) and different bed characteristics (TS and PS carbopol beds, TS and PS laponite–carbopol beds) were carried out in order to investigate their effects on the erosion behavior.

First of all, careful visual observations during all the experiments lead to a first macroscopic description of cohesive bed

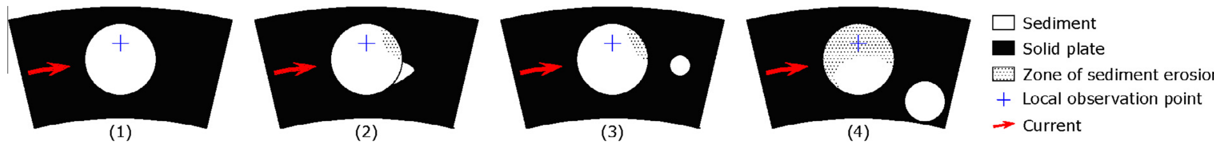

Fig. 10. Principal evolutions of PS cohesive beds (top view): steps 1–2 for the carbopol gel (t = 9200 s), steps 1–4 for the laponite–carbopol gel (t = 8500 s).

evolution. Concerning the TS carbopol and laponite–carbopol beds, no specific manifestations occurred besides vibratory motions of bed surface for an observation time of more than 5000 s. Such dynamics were stronger for the laponite–carbopol system. Thus, the bottom shear stress induced by the current was only able to deform both cohesive beds elastically at different levels. But the deformation in the whole bed section is not uniform as it depends on the distribution of bottom shear stress.

In contrast, strong destabilizing phenomena were observed for the PS-type beds (Fig. 10). Bed structures, which were initially stable (step 1), started to vibrate under the influence of the turbulent flow before flowing (solid–liquid transition process) in some zones. At the end of the test with the PS carbopol bed (t = 9200 s), a small quantity of the gel was found on the edge of the solid plate in the downstream part of the circular section (step 2). It seems that this lump of gel slides over the wall of the solid plate from a high velocity region towards the inner wall of the flume before climbing and staying on the plate. That said the bottom shear stress in that zone, resulting from the coupling between hydrodynamic flow and bed geometry, slightly exceeds the mechanical strength of the bed. The affected zone is still far from the local visualization point at r_f = 139.5 mm marked by the "plus" symbol in Fig. 10. For the PS laponite–carbopol bed, more remarkable processes are observed and confirm that this material is more sensitive to destabilization than the carbopol gel. The second step appears much earlier and the stretched piece of gel is detached from the bed and transported by the current as well (step 3) at t < 1000 s. This means that the viscosity decreases with time under shear (thixotropy effect [24]) and causes an acceleration of the gel flow. The eroded material is transported as bed load near the inner wall as its density (1153 kg/m^3) is greater than the one of the WS-PO (821 kg/m^3). Indeed, this element must, in return, modify flow structures near the bottom. Other fractions of the gel are eroded one after another in this similar way. Then, these pieces of gel, flowing at different speeds due to their different weights, coalesce to form a bigger one (step 4). After about 4200 s, the material remaining in the circular section does not evolve anymore and the region where the gel is eroded is crescent-shaped. It seems that the remaining gel in the well is blocked by the arc wall of the solid plate as the bed shear stress in that zone is not high enough. These are signs of shear localization within the sample. In summary, there exists a clear scenario of erosion mechanisms once the bed shear stress exceeds the

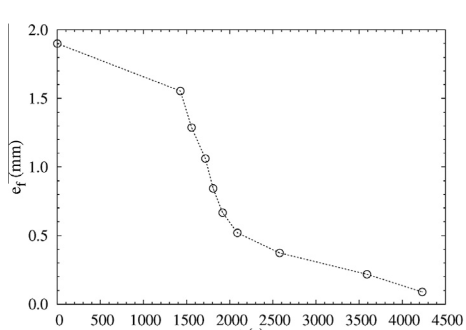

Fig. 11. Temporal evolution of the thickness of the PS laponite–carbopol bed at r_f = 139.5 mm.

cohesive bed strength. The effects of bed characteristics are also revealed as the erosion is more critical for the laponite–carbopol gel and the PS-type bed. Since the mixed gel exhibits a more pronounced thixotropy, it is likely that this feature, due to organization and interaction between structural elements, plays a destabilizing role.

An attention should be paid to the test with the PS laponite–carbopol bed since solid–liquid transition processes also occur in the local visualization zone. Thus, it is interesting to analyze the temporal evolution of the bed thickness at this position. Fig. 11 shows that the bed thickness decreases slightly during the first period of about 1400 s, then sharply before slowing down with time. It attains a value of less than 0.1 mm at 4200 s. After that, it does not evolve anymore as the shear stress becomes weaker than the material strength. This observation also suggests that the shear stress decreases with depth inside the circular section.

In order to get a better understanding of material dynamics until failure occurs, we should focus on the data at the microscopic scale. For the PS laponite–carbopol bed, many tracer particles enter and leave the visualization window consecutively with time as the material flows. In this case, a series of particle trajectories with time are selected and connected together in order to get significant information for analyzing the solid–liquid transition behavior. For all the four tests, particle trajectories are globally similar to the trajectory (c) presented in Fig. 8. Results are directly analyzed via the evolution of particle displacement Δr with time (Fig. 12).

Once again, the flow onset regime leads to the same Δr evolution (Fig. 12a). Since the tests refer to same flow conditions (WS-PO at Re = 14,700) the characteristic time of this step is about constant ($t_{co} \approx 20$ s) but local responses of bed material are different as presumed macroscopically. Displacements are more important when flume test section occupied by the carbopol gel is partial, and in all cases for laponite–carbopol gel which is easily disturbed for these conditions. The particle displacement during the steady-state flow regime increases as a power law of time until the end of the test (phase 3). However for carbopol gel, Δr values are about 3 times smaller for the TS bed gel than those for the PS bed. For the later, there even exists a slight acceleration of particle displacement from 2500 s (phase 4). Thus, the gel placed in the confined circular section is deformed stronger in the elastic domain. In contrast, for the PS laponite–carbopol bed, the curve is more specific and highlights the transition from a solid-like to a liquid-like state as the displacement increases sharply (phase 4), although not regularly, just after about 30 s. Furthermore, the Δr value at t = 1300 s is up to 8 mm which is over 20 times greater than those for the other three tests. From the physical point of view, the material in the observation zone starts to flow shortly after the flow regime is developed, but its velocity is not constant. Thus, the mixed gel is more sensitive to erosion than the carbopol gel, especially, when it is placed in the confined circular section. These local data are consistent with the macroscopic visual observations.

The dimensionless particle displacement profiles illustrated in Fig. 12b are obtained by using the corresponding characteristic coordinates (t_c, Δr_c). All the data collapse onto a single master curve during the first period of about 20 s. This apparently underlines the same local dynamics in the elastic domain of cohesive bed. The profile of the test with the PS laponite–carbopol bed is

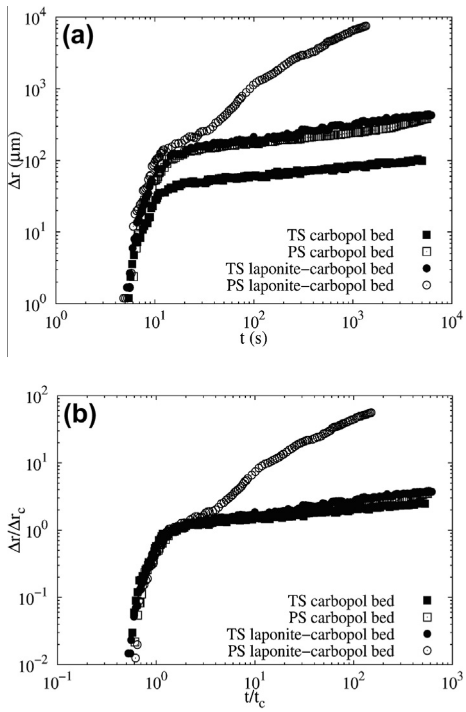

Fig. 12. (a) Temporal evolution of the particle displacement compared to its initial position during the creep step, (b) non dimensional particle displacement profiles during the creep step.

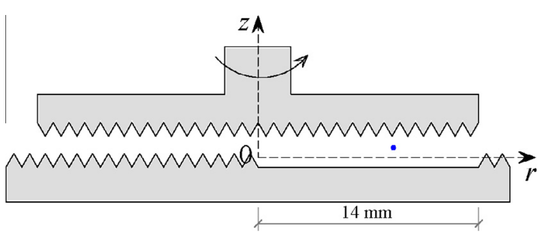

Fig. 13. Experimental configuration for rheometric creep tests in [38]: plate–plate geometry and local observation point at $r = 8.60$ mm and $z = 0.62$ mm.

well distinguished from the others as it is the only case that solid–liquid transition in the focused zone occurs.

4.3. Correlation between the shear stress measured with erosion and rheometric tests

One important question about bed shear stress that still remains concerns the interest of rheometric tests which give access to the yield stress. Is this latter parameter reliable in order to estimate critical bed shear stress associated to erosion? We can first claim from experiments that the critical shear stress for erosion is much smaller than rheometric yield stress value when exchanges at the bed interface exist. This is mainly due to perturbation of top bed layers which thus exhibit different properties from the bulk. Perturbation kinetic depends on material properties and flow conditions. As rheometric tests are not able to use representative samples of the top layers, only correlations could be obtained between critical bed shear stress and yield stress value of the bulk. In natural conditions, the situation is more complex as concentration of bed materials is not homogeneous due to consolidation phenomena. This interpretation is globally consistent with the findings presented in [10] and [18] for other cohesive materials knowing that the criteria used to determine both stresses

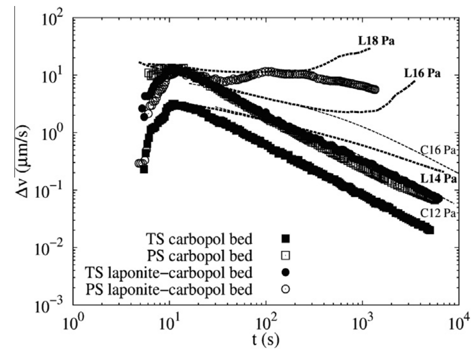

Fig. 14. Temporal evolution of the particle velocity compared to its initial position. The symbols represent the data of erosion tests with the WS-PO as driving fluid whereas the dashed curves represent the rheometric creep results (C for the carbopol gel and **L** for the laponite–carbopol gel).

have an effect on the correlations. It has been also reported that the critical stress for erosion can be a few orders of magnitude smaller than the macroscopic strength of the soil [43].

The erosion tests with the WS-PO solution allow us to deal with homogeneous bed materials which is well suited for a direct comparison with rheometric tests. Since various existing methods for determining the yield stress [23] and the critical stress for erosion [43] generally give very different results, micro-scale observations are mandatory to obtain a more accurate evaluation. As such, rheometric creep tests coupled with local particle tracking within the gap were conducted to characterize material flow/deformation. Two rough plates with 14 mm radius and 1 mm apparent gap were used (Fig. 13). The unique observation point is located at $r = 8.60$ mm and $z = 0.62$ mm. Since we focus on a zone with maximal bed shear stress for the erosion tests, the rheometric data in [38] should be transformed to obtain those at the edge of the rotating plate where the shear velocity is the greatest. This is done by considering that the velocity evolves linearly with z and r axes (no shear bands), which is correct when the sample undergoes homogeneous deformation or laminar flow. The results of both types of test are presented under the form of the temporal evolutions of the particle velocity calculated from its initial position ($\Delta v = \Delta r/\Delta t$) (Fig. 14).

Each velocity profile of erosion test exhibits a maximum at about 10 s previously noted as t_c. But it is more important to understand material responses during the apparent steady-state turbulent regime ($t > 20$ s). All the evolutions, except that of the test with the PS laponite–carbopol bed, are globally similar as the particle velocity decreases monotonously with time. This underlines the elastic shear strain of bed material (steady state creep phase) which is coherent in regard to the rheometric results as those three curves are mostly below the ones of the tests with applied stresses close to the yield stress (16 Pa for the carbopol gel and 14 Pa for the mixed gel). This also allows us to estimate that the bed shear stress for the PS carbopol bed is about 12 Pa, which is greater than the one for the TS carbopol bed but close to the one for the TS laponite–carbopol bed. Concerning the PS laponite–carbopol bed, the velocity seems to fluctuate around a constant value. The minimum of the curve at $t \approx 30$ s corresponds to the point that the material starts to flow (*i.e.*, failure occurs). Thus, the corresponding time should be defined as the solid–liquid transition time, which basically decreases with the level of shear stress. Rheometric measurements show that such characteristic time increases exponentially with the inverse of applied stress [30,38]. The slowdown of flow velocity in the last part of the curve is due to time-varying shear localization and ongoing processes of the sample. Since the velocity profile stays between those obtained at 16 Pa and 18 Pa for the same material, we can suppose that the bed shear stress is around this range which exceeds the yield stress value. Hence, it seems that there is an agreement between the erosion and rheometric experiments in term of the material strength, *i.e.*, the critical stress for erosion and the rheometric yield stress are about equivalent. Moreover, the estimated local bed shear stress values of the four tests are different although the same flow conditions are applied (*e.g.*, same ring rotating speed). This explains that the use of macroscopic flow conditions alone may not be sufficient to accurately estimate local bed shear stress which is interdependent with bed characteristics.

5. Discussion

The experiments with the miscibility and immiscibility conditions lead to reach the same remarks on the effects of bed characteristics on the erosion behavior. Firstly, the sample put in the confined circular section (PS bed) is more critical to destabilization (deformation or flow) than the one filled in the whole section of the flume (TS bed). The comparison between results obtained with both bed sections makes sense because all the samples are reproducible and the sediment behavior is explored locally, which can reduce the measurement errors underlined in [7,9]. Secondly, structural organization of bed material has a very significant effect as solid–liquid transition dynamics take place more rapidly for the laponite–carbopol gel than for the carbopol gel irrespective of the bed section (Figs. 7 and 12). Indeed, the former exhibits a more brittle-like behavior as its elastic modulus, viscous modulus and yield stress values are all more or less smaller than those of the latter. The mixed gel also has a much stronger thixotropic feature and higher water content. Although our materials cannot fully match real complex cohesive sediments, the results confirm that several parameters must be taken into account to accurately predict the erosion which is difficult and that the key parameter controlling the erosion is cohesive bed properties which thus should be characterized as much as possible. Moreover, local measurements allow us to better describe and quantify erosion processes of cohesive bed.

The experiments with the presence of cohesive bed–flume fluid exchanges are similar to natural conditions. Such phenomena tend to reduce the initial strength of bed material which is undoubtedly favorable for erosion to occur. The erosion process can take place more and more quickly with time even for an imposed constant hydrodynamic flow (Fig. 7). A conclusion is that the value of the critical stress for erosion depends on the observation time. Indeed, the protocol of mechanical solicitation (*e.g.*, constant stress and stress sweep tests) controls the evolution of the erosion rate [7,9]. At the local scale, the very first dynamics of both bed materials are similar since the tracer particles move relatively in the direction of the current, following the start-up of ring rotation. After that short time, particle dynamics are principally related to structural organization of cohesive bed regardless of its section. Concerning the carbopol gel, the erosion process is stripping-like as particles are individually and continuously detached from the bed then transported by the turbulent flow. As for the laponite–carbopol gel, having more complex structures due to a mixture of clay and polymeric elements, motions of all the particles are very disordered at the visualization scale. In addition, three particular erosion modes, including stripping, aggregate fragmentation and mass erosion, are encountered (Figs. 5 and 7). The first two types can appear simultaneously at different locations but the second one is much more remarkable. The aggregate formation should be mainly related to laponite clay structure as its concentration (0.45 wt.%) in the mixed system is nearly 4 times higher than the one of carbopol (0.12 wt.%). Material structure also depends upon the preparation protocol (*e.g.*, order of the addition of material components) as shown in [42] for other types of clay. Mass erosion, which is well defined in literature [11,17], appears when the bed becomes sufficiently thin ($e_f \approx 1.1$ mm for the TS bed and 0.6 mm for the PS bed). The origin of this dramatic process can be ascribed to two key factors. Firstly, the density and the yield stress of the mixed gel, which are slightly smaller than those of the carbopol gel, are reduced more greatly with time due to physicochemical interaction with the flowing driving fluid. Secondly, the mixed gel presents strong solid–liquid transition dynamics above the yield stress and a very pronounced thixotropic character leading to a decrease in viscosity under shear (Fig. 1). It should be reminded that the yield stress and the thixotropy of a fluid originate from the same basic physics [24]. In summary, the nature of material itself (compositions and interaction between them) is the main source of various physical breakdown mechanisms. Perhaps, the aspect of bed material-flume fluid exchanges can be analyzed further by considering samples permeability.

When bed material is immiscible with flume fluid, its initial mechanical strength remains unchanged. The cohesive bed thus can hold up high shear stress against erosion. The flow velocity and viscosity of driving fluid play a similar role in increasing the stress level since the bed undergoes bigger strain (*i.e.*, the tracer particle moves over a larger distance) when the flow is more turbulent or the flume fluid is more viscous (Fig. 8). The presence of eroded materials could also modify the original viscosity as well as the flow regime in the flume. The effects should be similar or even more dramatic in the case of miscibility. Thus, the shear stress should be measured instantaneously and locally as long as remarkable sediment processes occur. For the same imposed hydrodynamic conditions, the geometry and properties of cohesive bed also have repercussions on local bed shear stress, thus local erosion behavior (Figs. 9 and 12). When the bed shear stress is below a critical value, the material is elastically deformed (*i.e.*, the particle moves slowly in a similar direction as the flow) and can eventually age (*i.e.*, the particle moves very slowly in a direction transverse to the flow) after a certain time. Otherwise, the material flows as failure occurs (*i.e.*, the particle moves quickly in a similar direction as the flow). According to global observations for PS beds (Fig. 10), erosion mechanisms respect a specific scenario: lump of material at the most downstream part of the circular section climbs the solid plate then stretches out before breaking down and being transported as bed load. Furthermore, the material only flows in some regions but remains solid elsewhere. This is consistent with shear localization feature as the bed shear stress is higher than the material strength in some areas but lower elsewhere. These results suggest that the circular form of the bed naturally modifies hydrodynamic flow structures near the bottom which can be critical for erosion.

6. Conclusions

The present study, using a new approach by combining flume measurements with a particle tracking technique, has allowed us to describe different processes of transparent cohesive bed from elastic deformation to failure. Investigations at the microscopic scale for erosion flume tests are the originality of this work.

The miscibility between the sample and the flume fluid plays a significant role as bed exchanges could exist or not. In case of exchanges at the bed interface, it leads to the weakening of bed mechanical properties, which satisfies the erosion. Conversely, in the case of immiscibility, the cohesive bed remains homogeneous and is much more resistant to erosion as the critical stress is important and comparable with the rheometric yield stress. Shear localization (inhomogeneous strain) is also observed as bed failure only occurs in some areas where the bed shear stress is the highest and exceeds the material strength. In the zones with low shear stress, the material is only deformed elastically, *i.e.*, the bonds between the particles are not broken. Tracer particle dynamics within the bed are similar during an early stage, but the failure scenarios are totally different between the tests with the miscibility and immiscibility cases. We can define, in a more objective way, the erosion of a cohesive bed as the transition from a viscoelastic solid to a liquid or flowing state. In addition, the erosion depends on the internal structures of the sample associated with its mechanical behavior (*e.g.*, strength and thixotropy) as various dynamics are observed for both studied systems. The measurement section also has an impact, even for the same sample and global experimental conditions, as it is able to modify the local bed shear stress. The processes in a cohesive bed as well as the erosion rate can change with time. Therefore, the observation time for mechanical solicitation can be a critical parameter, which is rarely seen mentioned in the literature for the estimation of the erosion threshold.

More importantly, we can assume that the local bed shear stress can vary with time and results from the coupling between the driving fluid and cohesive bed conditions. In any case, data at the local scale are necessary for accurately estimating the critical stress for erosion as well as exploring the cohesive bed failure.

Most erosion flumes were designed to measure directly the concentration of suspended materials for different shear stress values according to a desired protocol. However, our instrument is more specific because it allows us to observe the very earlier processes of the sediment at the local scale. Indeed, this study does not only confirm some existing findings in the literature in a more detailed manner with small scale investigation, but also reveals something new like the presence of shear localization within the bed. This work also brings to the attention the uncertainty of classical critical stress estimation using macroscopic data (*i.e.*, concentration of suspended materials), which can be very important.

Certainly, it is very interesting, although difficult, to improve our current experimental system so that the local shear stress can be measured precisely and instantaneously. This may enable us a possibility to provide a new erosion equation, especially for the small scale. After that, similar work focusing on "non transparent" natural cohesive sediments can be an interesting subject of future research, but a more specific measurement system must be set up.

References

[1] Le Hir P, Monbet Y, Orvain F. Sediment erodibility in sediment transport modeling: can we account for biota effects?. Cont Shelf Res 2007;27:1116–42. http://dx.doi.org/10.1016/j.csr.2005.11.016.

[2] Lundkvist M, Grue M, Friend PL, Flindt MR. The relative contributions of physical and microbiological factors to cohesive sediment stability. Cont Shelf Res 2007;27:1143–52. http://dx.doi.org/10.1016/j.csr.2006.01.021.

[3] Pouv KS, Besq A, Guillou S. Rheometric study for elaborating transparent model of cohesive sediments for local investigations of erosion behaviour. Rev Paralia 2012;5:1–14. http://dx.doi.org/10.5150/revue-paralia.2012.001.

[4] Andersen TJ. Seasonal variation in erodibility of two temperate, microtidal mudflats. Estuar Coast Shelf Sci 2001;53:1–12. http://dx.doi.org/10.1006/ecss.2001.0790.

[5] Tolhurst TJ, Defew EC, de Brouwer JFC, Wolfstein K, Stal LJ, Paterson DM. Small-scale temporal and spatial variability in the erosion threshold and properties of cohesive intertidal sediments. Cont Shelf Res 2006;26:351–62. http://dx.doi.org/10.1016/j.csr.2005.11.007.

[6] Mitchener H, Torfs H. Erosion of mud/sand mixtures. Coast Eng 1996;29:1–25. http://dx.doi.org/10.1016/S0378-3839(96)00002-6.

[7] Tolhurst TJ, Black KS, Paterson DM, Mitchener HJ, Termaat GR, Shayler SA. A comparison and measurement standardisation of four in situ devices for determining the erosion shear stress of intertidal sediments. Cont Shelf Res 2000;20:1397–418. http://dx.doi.org/10.1016/S0278-4343(00)00029-7.

[8] Widdows J, Friend PL, Bale AJ, Brinsley MD, Pope ND, Thompson CEL. Inter-comparison between five devices for determining erodability of intertidal sediments. Cont Shelf Res 2007;27:1174–89. http://dx.doi.org/10.1016/j.csr.2005.10.006.

[9] Sanford LP. Uncertainties in sediment erodibility estimates due to a lack of standards for experimental protocols and data interpretation. Integr Environ Assess Manag 2006;2:29–34. http://dx.doi.org/10.1002/ieam.5630020106.

[10] Otsubo K, Muraoka K. Critical shear stress of cohesive bottom sediments. J Hydraulic Eng 1988;114:1241–56. http://dx.doi.org/10.1061/(ASCE)0733-9429(1988)114:10(1241).

[11] Amos CL, Daborn GR, Christian HA, Atkinson A, Robertson A. In situ erosion measurements on fine grained sediments from the Bay of Fundy. Mar Geol 1992;108:175–96. http://dx.doi.org/10.1016/0025-3227(92)90171-D.

[12] Houwing EJ, van Rijn LC. In Situ Erosion Flume (ISEF): determination of bed-shear stress and erosion of a kaolinite bed. J Sea Res 1998;39:243–53. http://dx.doi.org/10.1016/S1385-1101(98)00007-0.

[13] Jepsen R, Roberts J, Lick W. Effects of bulk density on sediment erosion rates. Water Air Soil Pollut 1997;99:21–31.

[14] Jacobs W, Le Hir P, Van Kesteren W, Cann P. Erosion threshold of sand–mud mixtures. Cont Shelf Res 2011;31:14–25. http://dx.doi.org/10.1016/j.csr.2010.05.012.

[15] Pope ND, Widdows J, Brinsley MD. Estimation of bed shear stress using the turbulent kinetic energy approach – A comparison of annular flume and field data. Cont Shelf Res 2006;26:959–70. http://dx.doi.org/10.1016/j.csr.2006.02.010.

[16] Kim SC, Friedrichs CT, Maa PY, Wright LD. Estimating bottom stress in tidal boundary layer from acoustic doppler velocimeter data. J Hydraulic Eng – ASCE 2000;126:399–406. http://dx.doi.org/10.1061/(ASCE)0733-9429(2000)126:6(399).

[17] Winterwerp JC, Van Kesteren WGM. Introduction to the physics of cohesive sediment in the marine environment. 1st ed. Amsterdam: Elsevier Science; 2004.

[18] Migniot C. Bedding-down and rheology of muds (Part 2). Houille Blanche 1989;2:95–111. http://dx.doi.org/10.1051/lhb/1989006.

[19] van Kessel T, Blom C. Rheology of cohesive sediments: comparison between a natural and an artificial mud. J Hydraulic Res 1998;36:591–602. http://dx.doi.org/10.1080/00221689809498611.

[20] Pantet A, Robert S, Jarny S, Kervella S. Effect of coarse particle volume fraction on the yield stress of muddy sediments from Marennes Oléron Bay. Adv Mater Sci Eng 2010;2010:1–6. http://dx.doi.org/10.1155/2010/245398.

[21] Aubry T, Razafinimaro T, Silva Jacinto R, Bassoulet P. Rheological properties of a natural estuarine mud. Appl Rheol 2003;13:142–9. http://dx.doi.org/10.3933/ApplRheol-13-142.

[22] Huang Z, Aode H. A laboratory study of rheological properties of mudflows in Hangzhou Bay, China. Int J Sediment Res 2009;24:410–24.

[23] Berlamont J, Ockenden M, Toorman E, Winterwerp J. The characterization of cohesive sediment properties. Coast Eng 1993;21:105–28. http://dx.doi.org/10.1016/0378-3839(93)90047-C.

[24] Møller PCF, Mewis J, Bonn D. Yield stress and thixotropy: on the difficulty of measuring yield stresses in practice. Soft Matter 2006;2:274–83. http://dx.doi.org/10.1039/B517840A.

[25] Piau JM. Carbopol gels: elastoviscoplastic and slippery glasses made of individual swollen sponges: meso- and macroscopic properties, constitutive equations and scaling laws. J Non-Newton Fluid Mech 2007;144:1–29. http://dx.doi.org/10.1016/j.jnnfm.2007.02.011.

[26] Ha HK, Maa JPY. Evaluation of two conflicting paradigms for cohesive sediment deposition. Mar Geol 2009;265:120–9. http://dx.doi.org/10.1016/j.margeo.2009.07.001.

[27] Coussot P. Rheophysics of pastes: a review of microscopic modelling approaches. Soft Matter 2007;3:528–40. http://dx.doi.org/10.1039/B611021P.

[28] Ovarlez G, Rodts S, Chateau X, Coussot P. Phenomenology and physical origin of shear localization and shear banding in complex fluids. Rheol Acta 2009;48:831–44. http://dx.doi.org/10.1007/s00397-008-0344-6.

[29] Coussot P, Tocquer L, Lanos C, Ovarlez G. Macroscopic vs. local rheology of yield stress fluids. J Non-Newton Fluid Mech 2009;158:85–90. http://dx.doi.org/10.1016/j.jnnfm.2008.08.003.

[30] Caton F, Baravian C. Plastic behavior of some yield stress fluids: from creep to long-time yield. Rheol Acta 2008;47:601–7. http://dx.doi.org/10.1007/s00397-008-0267-2.

[31] Divoux T, Tamarii D, Barentin C, Manneville S. Transient shear banding in a simple yield stress fluid. Phys Rev Lett 2010;104:208301. http://dx.doi.org/10.1103/PhysRevLett.104.208301.

[32] Rodts S, Baudez JC, Coussot P. From "discrete" to "continuum" flow in foams. Europhys Lett 2005;69:636–42. http://dx.doi.org/10.1209/epl/i2004-10374-3.

[33] Oppong FK, Rubatat L, Frisken BJ, Bailey AE, de Bruyn JR. Microrheology and structure of a yield-stress polymer gel. Phys Rev E 2006;73:1–9. http://dx.doi.org/10.1103/PhysRevE.73.041405.

[34] Mongondry P, Tassin JF, Nicolai T. Revised state diagram of laponite dispersions. J Colloid Interface Sci 2005;283:397–405. http://dx.doi.org/10.1016/j.jcis.2004.09.043.

[35] Willenbacher N. Unusual thixotropic properties of aqueous dispersions of laponite RD. J Colloid Interface Sci 1996;182:501–10. http://dx.doi.org/10.1006/jcis.1996.0494.

[36] Mourchid A, Lecolier E, Van Damme H, Levitz P. On viscoelastic, birefringent, and swelling properties of laponite clay suspensions: revisited phase diagram. Langmuir 1998;14:4718–23. http://dx.doi.org/10.1021/la980117p.

[37] Tiu C, Guo J, Uhlherr PHT. Yielding behaviour of viscoplastic materials. J Ind Eng Chem 2006;12:653–62.
[38] Pouv KS. Vers un lien entre proprieties mécaniques de sediments cohésifs et leur érodabilité, [Ph.D. thesis]. Université de Caen; 2011. [in French].
[39] Araújo MAVC, Teixeira JCF, Teixeira SFCF. Application of laser anemometry for measuring critical bed shear stress of sediment core samples. Cont Shelf Res 2008;28:2718–24. http://dx.doi.org/10.1016/j.csr.2008.09.011.
[40] Sbalzarini IF, Koumoutsakos P. Feature point tracking and trajectory analysis for video imaging in cell biology. J Struct Biol 2005;151:182–95. http://dx.doi.org/10.1016/j.jsb.2005.06.002.
[41] Uhlherr PHT, Guo J, Tiu C, Zhang XM, Zhou JZQ, Fang TN. The shear-induced solid–liquid transition in yield stress materials with chemically different structures. J Non-Newton Fluid Mech 2005;125:101–19. http://dx.doi.org/10.1016/j.jnnfm.2004.09.009.
[42] Besq A. Ecoulements laminaires de suspensions de bentonites industrielles, [Ph.D. thesis]. Université de Poitiers; 2000. p. 238.
[43] Partheniades E. Cohesive sediments in open channels. Burlington: Elsevier Science; 2009.
[44] Moyers-Gonzalez M, Frigaard IA, Nouar Chérif. Stable two-layer flows at all Re; visco-plastic lubrication of shear-thinning and viscoelastic fluids. J Non-Newton Fluid Mech 2010;165:1578–87. http://dx.doi.org/10.1016/j.jnnfm.2010.08.005.
[45] Hormozi S, Martinez DM, Frigaard IA. Stable core-annular flows of viscoelastic fluids using the visco-plastic lubrication technique. J Non-Newton Fluid Mech 2011;166:1356–68. http://dx.doi.org/10.1016/j.jnnfm.2011.08.013.
[46] Møller PCF, Fall A, Bonn D. Origin of apparent viscosity in yield stress fluids below yielding. Europhys Lett 2009;87:38004. http://dx.doi.org/10.1209/0295-5075/87/38004.
[47] Guillou S, Thiébot J, Chauchat J, Verjus R, Besq A, Nguyen DH, Pouv KS. The filling dynamics of an estuary: from the process to the modelling. In: Manning A, editor. Sediment transport in aquatic environments. INTECH; 2011, ISBN 978-953-307-586-0. p. 125–46 [chapter 6].
[48] Thiébot J, Guillou S, Brun-Cottan JC. An optimisation method for determining permeability and effective stress relationships of consolidating cohesive sediment deposits. Cont Shelf Res 2011;31(Suppl. 1):S117–23. http://dx.doi.org/10.1016/j.csr.2010.12.004.
[49] Van LA, Phan Van Bang D. Hindered settling of sand/mud flocs mixtures: from model formulation to numerical validation. Adv Water Resour 2013;53:1–11. http://dx.doi.org/10.1016/j.advwatres.2012.09.009.
[50] Chauchat J, Guillou S, Pham Van Bang D, Nguyen KD. Modelling sedimentation–consolidation in the framework of a one-dimensional two-phase flow model. J Hydraulic Res 2013;51:293–305. http://dx.doi.org/10.1080/00221686.2013.768798.
[51] Amoudry LO. Assessing sediment stress closures in two-phase sheet flow models. Adv Water Resour 2012;48:92–101. http://dx.doi.org/10.1016/j.advwatres.2012.03.011.
[52] Revil-Bauchard T, Chauchat J. A two-phase model for sheet flow regime based on dense granular flow rheology. J Geophys Res 2013;118:1159–73. http://dx.doi.org/10.1029/2012JC008306.
[53] Nguyen KD, Guillou S, Chauchat J, Barbry N. A two-phase numerical model for suspended-sediment transport in estuaries. Adv Water Resour 2009;32:1187–96. http://dx.doi.org/10.1016/j.advwatres.2009.04.001.
[54] Jha SK, Bombardelli FA. Toward two-phase flow modeling of non dilute sediment transport in open channels. J Geophys Res 2010;115:F3. http://dx.doi.org/10.1029/2009JF001347.
[55] Yeganeh-Bakhtiary A, Kazeminezhad MH, Etemad-Shahidi A, Baas JH, Cheng L. Euler–Euler two-phase flow simulation of tunnel erosion beneath marine pipelines. Appl Ocean Res 2011;33(2):137–46. http://dx.doi.org/10.1016/j.apor.2011.01.001.
[56] Yu Z, Shao X. A direct-forcing fictitious domain method for particulate flows. J Comput Phys 2007;227(1):292–314. http://dx.doi.org/10.1016/j.jcp.2007.07.027.